

Chapter 5

Observations of internal tides in the Mozambique Channel

5.1 Introduction

Internal tides can be found nearly everywhere in the ocean. They are generated by barotropic tides over topography. It is thought that this conversion of barotropic to baroclinic tides (internal tides) is a major sink for the barotropic tidal energy (Sjöberg & Stigebrandt, 1992). The obliquely propagating internal waves are in turn subject to reflections and scattering. As we have seen in the previous chapters, reflection may lead to local concentration of energy, until the linear approximation breaks down and energy is transferred to even smaller scales. Thus they must form an important link in the process of energy transfer from large scale tidal motions to smaller scales.

Ultimately, the cascade to smaller scales makes the energy available for mixing. Where and by which mechanism mixing occurs in the ocean is a topic of active research (Munk & Wunsch, 1998). Observed diffusivity values in the open ocean are too low to account for the mixing rates that are necessary to maintain the global circulation. This implies that local mixing rates must be even higher than the required global average. Indeed, estimates have been made of the amount of dissipation of tidal energy. Satellite sea surface height measurements provide an accurate global tidal field, that can be used to feed numerical models that calculate the corresponding barotropic currents. These in turn can be used to study the effects of interaction with topography (Egbert & Ray, 2001), like friction and generation of internal tides. Where internal tides reflect at the bottom and especially where internal waves are parallel to the slope, mixing rates should be high. Thus, areas with strong topography are considered as sites of strong mixing. Submarine canyons play a special role, as they may act as a trap for internal waves (Petruncio *et al.*, 1998).

But the coverage of the ocean by in situ measurements is poor and observations are not equally spread. Observations are mainly in the generation areas, where the direct beams can be observed to large depth (Pingree & New, 1991), or completely confined to the shelf area. Recent examples include the upper 100 m above West Florida Continental Shelf (Leaman,

1980), the upper 1200 m across the Australian Shelf (Holloway *et al.*, 2001), the upper 500 m across the Californian shelf (Lerczak *et al.*, 2003), and the upper 700 m above the shelf in the Bay of Biscay (Lam *et al.*, 2003). In the open ocean, internal waves are observed hundreds of kilometres away from their generation area, as found from satellite altimetry (Ray & Mitchum, 1997) and direct observations (Morozov, 1995). They obviously survive a considerable number of reflections, although their beam-like nature is found to disappear, justifying the use of only the low modes in the open ocean.

Little is known about the structure of the internal wave field in enclosed basins. The existence of internal seiches in a lake was investigated by (Fricker & Nepf, 2000). Attention has been paid to the Faeroe-Shetland channel (van Veldhoven, 2000; Gerkema, 2002), but observations of the internal wave field with sufficient spatial resolution are still lacking.

In this chapter, the distribution of internal wave energy in the Mozambique Channel is studied. This narrow sea strait between Mozambique and Madagascar has a steep topography on the scale of internal waves and a reasonably strong surface tide, with elevations of about 1 m for lunar (M_2) and solar (S_2) semidiurnal tides (LeProvost, 2001), which makes the area favourable for the generation of internal tides. The observations consist of a year and a half-long moored current meter records and five 13-hour yo-yo measurements in the narrowest region of the Mozambique Channel. The mooring array was not specifically designed for the observations of internal tides, as it was primarily used to study the large scale currents in the channel (Agulhas Current Sources EXperiment, further referred to as ACSEX, see Ridderinkhof & de Ruijter, 2003). The horizontal separation of the current meters is larger than the wavelength, so too large to directly relate their records. Therefore a ray-tracing model and a numerical internal-tide generation model, in which the observed stratification and topography were incorporated, are used to support interpretation of the observations.

The structure of this chapter will be as follows. First, the most important currents and the stratification of the channel will be described briefly. A simple ray-tracing program is used to calculate the paths followed by the wave rays. A more sophisticated internal-tide generation model is used to predict the distribution of wave energy and the relative phase field for the cross section of the channel. Next the results from the yo-yo stations are shown and compared with the numerical tide generation model. Then the mooring section will be presented and the treatment of the data will be discussed. The barotropic and baroclinic currents are separated using harmonic analysis. After that, we will restrict ourselves to semidiurnal internal tide signals. The long records exhibited strong variability (intermittency). Amplitude and phase changes in the vertical of two moorings were monitored to describe the variation and vertical structure of the internal waves. To classify the full time records, differences and main features of the spectra are pointed out and the average energy in spectral bands is calculated. The results are compared with results from the numerical internal-tide generation models for interpretation.

5.2 Description of the Mozambique channel

The Mozambique Channel is a deep sea strait in between the African continent and Madagascar. It is only 370 km wide on its narrowest part, with a depth of up to 2700 m next to the Davie Ridge, over which the depth decreases rapidly to 2000 m. The bathymetry and

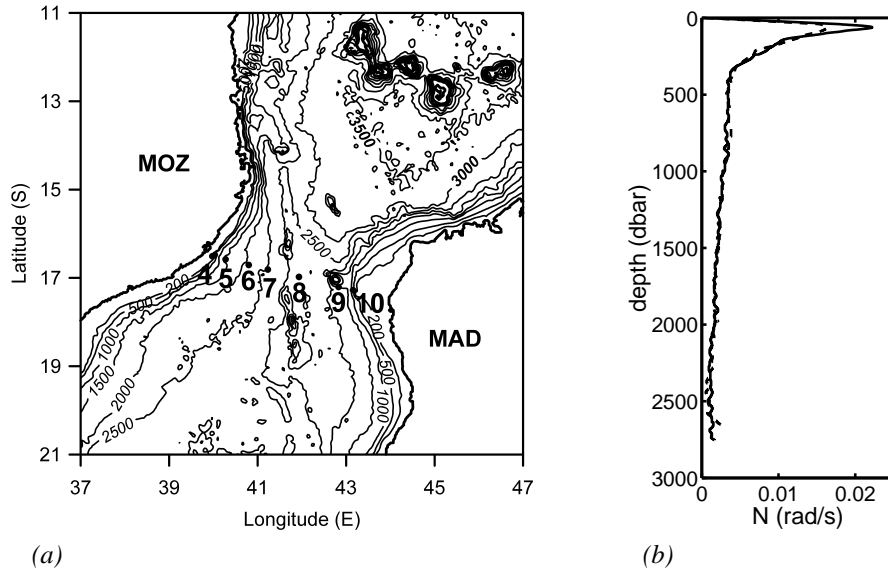


Figure 5.1: (a) Map of the research area. The mooring positions are indicated by the black dots. The islands around 12° S are the Comores. (b) Representative Brunt-Väisälä frequency for 2000 (dashed) and 2001 (solid), as determined from the ensemble of CTD-stations.

mooring locations are shown in figure 5.1(a). Little has been published about the flow in the Mozambique Channel. Schuman (1998) and DiMarco *et al.* (2002) did not find a persistent flow: the flow in the channel is variable, possibly due to the presence of eddies. Their observations were a collection of snapshots of the local flow field. Especially from the central part of the Mozambique Channel hardly any observation was available.

In the ACSEX-program, two cruises were undertaken with the Dutch Research Vessel *Pelagia* to study the flow in the channel, in March-April 2000 and 2001. An array of current meter moorings has been operating for more than a year and a half in the narrowest part of the channel. The data were completed with vessel mounted ADCP (Acoustic Doppler Current Profiler) and drifter data and several CTD (Conductivity-Temperature-Depth) sections. The present study is based on measurements that were done as part of the ACSEX-project. In addition to the current meter mooring and CTD-observations, yo-yo measurements were carried out to detect internal waves.

The large scale flow in the channel, based on these observations, is described in Ridderinkhof & de Ruijter (2003) and is briefly summarized here. It appears to be dominated by the southward passage of large anticyclonic eddies, with cross sections of about 350 km, which fill the Mozambique Channel at its narrowest part. They are formed in or slightly to the north of the region of the moorings and appear rather regularly, 4 to 5 per year. The eddies extend over the full water column with weakly depth-varying currents of more than 40 cm/s in the upper hundreds of metres. Near the African slope, at depths between 1500 and 2500 m, the Mozambique Undercurrent was observed, flowing northwards with a speed of about 4.5 cm/s.

The strength of the stratification is best represented by the Brunt-Väisälä-frequency N . It is defined according to

$$N^2(z) = -\frac{g}{\rho_0} \frac{d\rho_0}{dz} + \frac{\rho_0 g}{c_s^2}$$

where g represents gravity, directed against the vertical z , ρ_0 the density and c_s is the local sound speed in the water, as determined by pressure, temperature and salinity, accounting for compressibility effects. Based on CTD-sections of the two cruises, profiles of N were computed using running means over 16 decibar (dbar) in the vertical to avoid spikes in the derivatives.

Figure 5.2 shows the stratifications in the channel during the two cruises. The first cruise was during the passage of an eddy whereas there was no eddy present during the second cruise. During the passage of an eddy, the water in the middle of the basin is warmer and more saline, resulting in a depression of the isopycnals. Maybe even more important is the difference in the structure in the upper 300 m of the water column (see the enlargement in figure 5.2), with a much stronger stratification when the eddy is absent. In the absence of an eddy the pycnocline is much sharper and has an arch-like structure, especially in the western part of the channel, whereas in the presence of an eddy the structure of the pycnocline is more or less hollow and less pronounced. The change in stratification due to eddies probably dominates seasonal changes. At this latitude the seasonal variation in temperature, the most important factor in the formation of a seasonal pycnocline, is far less than at higher latitudes. In the lower part of the water column the values of N are nearly equal for the two cruises.

5.3 Internal wave models

The angle θ of the internal wave rays with the direction of gravity depends on the frequency of the wave ω , on $N(z)$ and on the local Coriolis parameter $f = 2\Omega \sin \phi$ with Ω the rotation frequency of the Earth and ϕ the geographical latitude. For a stratification that varies slowly with respect to the wave length of the internal waves, this angle is locally given by

$$\tan^2 \theta = \frac{N^2 - \omega^2}{\omega^2 - f^2} \quad (1)$$

The phase lines are parallel to the wave rays, the phase propagates in a direction perpendicular to the direction of energy propagation. They propagate in the same horizontal, but in the opposite vertical direction. The large scale eddies affected the stratification and therefore must affect the theoretical paths of the internal wave beams.

Two numerical models were used to study the internal wave field theoretically. These models use the observed topography and stratification. A horizontally uniform stratification has been used. This stratification is the average value for the part below the pycnocline, but for the upper part an artificial pycnocline peak is constructed, that has a peak value that is around the average peak value, at a depth that is around the average pycnocline depth. A pure horizontal average of the profiles of the different CTD-stations would have smoothed out the pycnocline and taking the profile of the deepest station as representative was not justified. Due to horizontal variations in the stratification, the predicted wave patterns will not be exact,

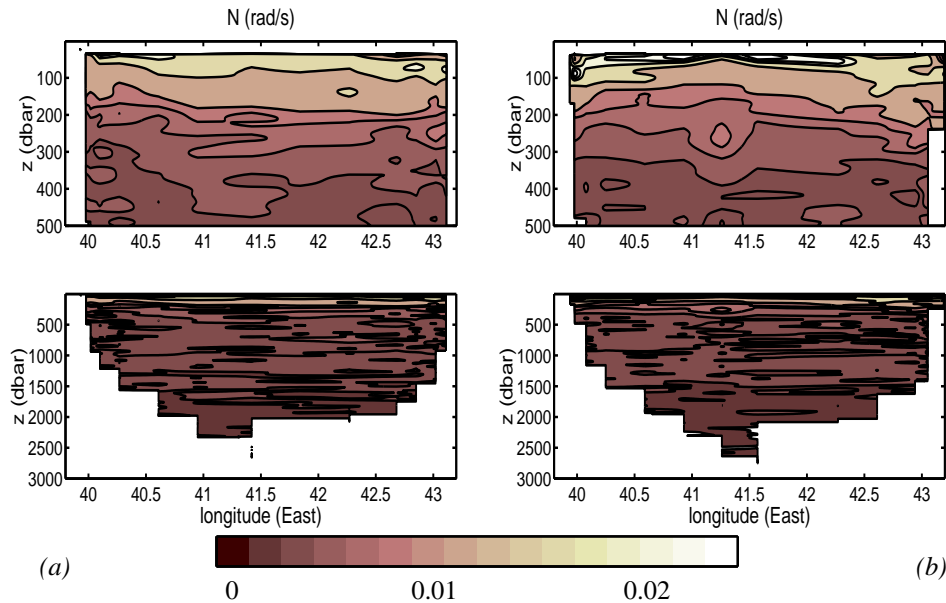


Figure 5.2: Brunt-Väisälä-frequency N (rad/s) for the CTD-profiles. The positions of the profiles can be determined from the block-shape channel depth representation. (a) 2000, in the presence of an eddy and (b) 2001 in absence of an eddy. The upper panel is an enlargement of the upper 500 m of the lower panel to illustrate the pycnocline structure.

but large scale features, like the number of reflections needed to cross the channel, will be represented correctly. The profiles are plotted in figure 5.1.

The first model is a simple two-dimensional ray-tracing model that indicates paths of wave rays. It only takes changes in direction due to changes in stratification and reflection at the bottom and surface into account. The steep, small-scale structures in the topography sometimes led to trapping or back-reflection of the wave. In reality, the waves will form beams of certain width and the fate of isolated rays is unimportant. Figure 5.3 shows the ray paths for M_2 for the two different stratification regimes. Only the rays starting from the Madagascar side are plotted for transparency. Wave rays cross the basin within 6 to 7 reflections. The two different stratifications lead to different ray paths, but major features are the same.

The ray-tracing model is a decent description under the restriction that the stratification does not change considerably on the scale of the wave length. In the pycnocline region this is not the case. Therefore, a more sophisticated model was used, that does not have this drawback and accounts for both the change in direction and internal reflections at the pycnocline, resulting in scattering of the waves. This internal-tide generation model (Gerkema, 2001) is a two-dimensional model, assuming along-slope uniformity. It again uses the observed topography and stratification $N(z)$ of the basin. The barotropic tide is converted into internal tides, using the cross-slope tidal flux. The tidal flux must be prescribed, but as the model is linear, its value only affects the absolute strength of the currents, not the relative. Ultimately the

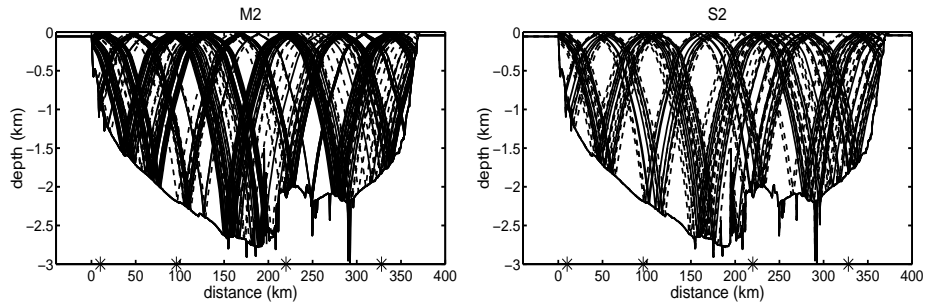


Figure 5.3: Ray paths starting on the Madagascar shelf (on the right), five upwards and five downwards, for the stratification with (dashed) and without eddy (solid). Left panel is for M_2 , right panel for S_2 . Stars indicate the yo-yo stations, that are discussed in the next section.

results were scaled as to roughly match the observed velocity amplitudes. The topography of the channel is transformed into a rectangular basin. In the vertical Chebishev-polynomials are used in a pseudo-spectral method. In the horizontal and for time integration a finite difference scheme has been used. A model run spanned 100 tidal periods, which appeared enough to overcome the transient response and find the equilibrium internal wave field. Although the amplitude was not completely constant, its variations were small and results did not change significantly. The results from this model will be shown together with the field observations.

5.4 Yo-yo results

During the 2001-cruise four 13 hour yo-yo measurements were carried out with a CTD-profiler over the full depth of the water column, close to the current meter mooring positions. Only the downcast measurements were used, as upcast measurements are less accurate due to the dragging of water by the CTD-frame. Since a single down and upcast takes nearly an hour at water depths of about 2000 m, the deep stations do not have a good time resolution (8-10 casts in 13 hours). This is still enough to capture semidiurnal waves but waves with higher frequencies cannot be resolved. Discrimination between the slightly different tidal components M_2 (lunar semidiurnal tide, period 12.42 hours) and S_2 (solar semidiurnal tide, period 12.00 hours), and components with smaller contributions to the spectrum, is not possible. There was one yo-yo station during the 2000-cruise, but since it is isolated in time its results were not used.

The excursions of the isotherms in time were analysed using harmonic analysis. Their amplitude A and phase ψ with respect to yearday 0 (January 1st 2000, 0 h00 UTC) were determined for the M_2 tidal frequency ω by calculating the fit to $z = A \cos(\omega t - \psi)$. In this convention, phase propagation is in the direction of increasing phase. The peak to trough amplitude is $2A$. Phase and energy propagation are opposite in the vertical direction. Thus locations of upward and downward propagating energy can be determined. The horizontal direction cannot be determined from observations in the vertical alone. When the same procedure was applied to the isopycnals nearly identical results were found.

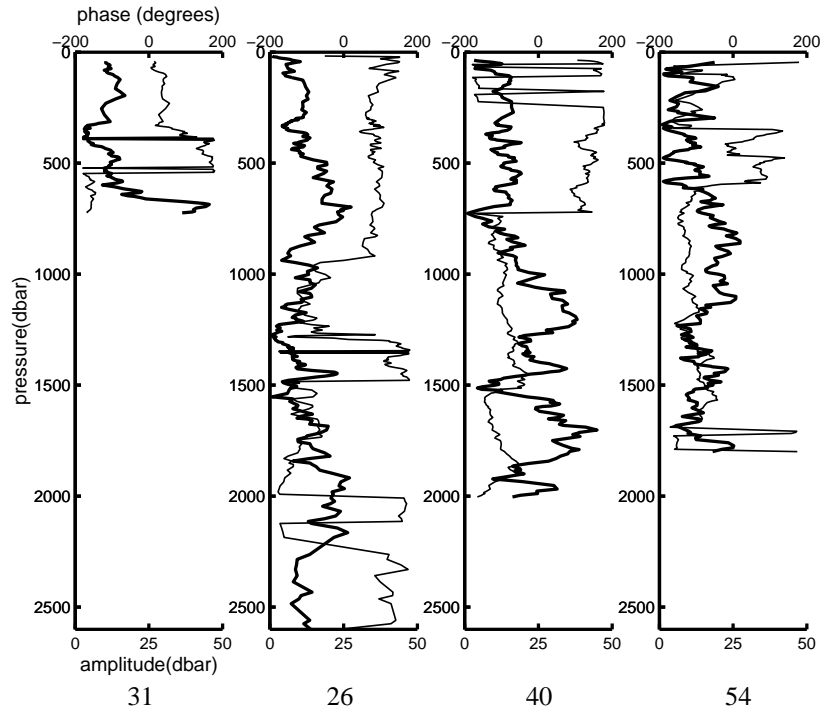


Figure 5.4: Amplitude (thick line) and phase (thin line) of harmonic analysis (M_2) of the isotherm displacement. The subplots are ordered such that they form a west-east cross section of the channel, their position is indicated in figure 5.5

In figure 5.4 the results are plotted. The fit of the isotherms to the M_2 -frequency is in general successful, around 80 % of the isotherm displacement in time is explained. Only at some depths this is not the case. Locations where this occurs can be identified from the low amplitudes in small depth intervals and this is often accompanied by a rapid phase change. At these locations internal motion is often present, but with larger (diurnal?) or shorter periods that cannot be resolved well. The phase jumps from about 180 to about -180 degrees must be interpreted as continuous phase changes, as the phase is defined on a cyclic scale.

In station 31 ($16^\circ 30.49'$ S, $40^\circ 0.71'$ E, depth 648 m) a large internal wave is detected near the bottom, with an amplitude of more than 40 dbar, implying an excursion of the isotherms of more than 80 m. This wave has a small extent in the vertical. The downward phase propagation implies upward travelling wave energy.

Station 26 ($16^\circ 49.26'$ S, $41^\circ 16.20'$ E, depth 2654 m) shows more modest internal wave activity with amplitudes of 20 dbar at a 'depth' of 700 dbar and around 2000 dbar. There is no clear phase propagation around 700 dbar, but phase changes abruptly at 1000 dbar. From 1300 to 1600 dbar the phase is increasing continuously, which points at upward energy propagation. Further downwards it decreases with a minimum around 2000 dbar and a sudden rise at 2200 dbar.

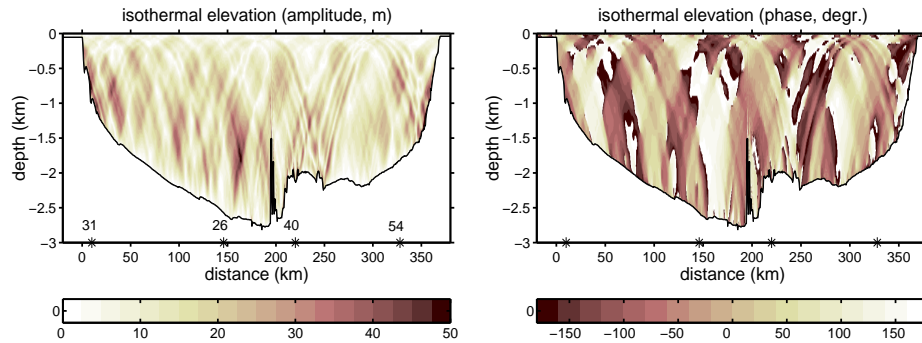


Figure 5.5: Amplitude and phase of isotherm displacement from the numerical internal-tide generation model. The absolute amplitude is arbitrary, depending on the barotropic flux.

Station 40 ($16^{\circ} 58.77' S$ $41^{\circ} 56.09' E$, depth 2008 m) has two large regions of strong wave activity with amplitudes around 40 dbar: around a depth of 1200 and 1700 dbar. They are separated by a region of low amplitude and a phase shift. In the regions of strong wave activity the phase is increasing slowly with depth, so the wave energy must be travelling upwards.

Station 54 ($17^{\circ} 12.34' S$ $42^{\circ} 49.67' E$, depth 1808 m) has modest internal wave activity, with a broad region around 900 dbar and two small regions around 1500 and 1800 dbar where the amplitude of the waves is around 20 dbar. There is a clear phase shift at 600 dbar. There is no evident phase propagation in the internal wave regions, so that no firm conclusions can be drawn about the direction of energy propagation.

The yo-yo stations are too far apart to follow a beam of internal waves in the horizontal. Reflection alters the phase, which hampers direct comparison between the stations. Furthermore, there is a week time difference between the first and the last yo-yo station, which may cause relative differences in amplitude due to the spring-neap cycle. Station 40 was during spring-tide, and indeed has internal waves with largest amplitude. The other stations are three to two days earlier (yearday 461, station 26, yearday 462, station 31) or three days later (yearday 467, station 54). Direct beams from the shelf were not identified.

The amplitude and phase of the isotherm displacement were calculated by the numerical tide generating model for the stratification observed in the 2001-cruise. It reproduces the large isotherm displacement at station 31, but not the large displacements at station 40. Overall, model isotherm displacements are larger at the Mozambique side of the channel, where they appear in large patches at mid-depth. The observed location of maximum isotherm displacement is represented fairly well. As for the phase, only relative phases can be compared. The locations of large phase transitions are more or less in accordance with the observations for station 26 (the large phase change around 1000 m depth) and 40. But for station 54 the phase change in the lower part of the water column is not observed, and for station 31 the direction of phase propagation is the other way round.

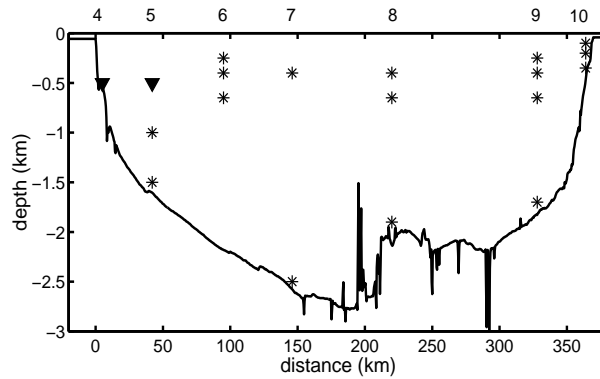


Figure 5.6: Distribution of current meters (stars) and upward looking ADCP's (triangles) over the Mozambique Channel. Numbers refer to mooring identification numbers.

5.5 Current meter results

Current meters that measure horizontal velocities were deployed in March-April 2000. After the first year of deployment, the moorings were surfaced, serviced and redeployed. In November 2001, the moorings were finally recovered with the British RV Charles Darwin. The exact locations and operation times of the instruments are displayed in table 5.1. Figure 5.1 indicates the geographical positions of the moorings. Figure 5.6 shows their vertical distribution over the channel. The ADCP's at the Mozambique-side cover the upper 500 m.

The current meters were connected to the bottom with long mooring cables. When the low-frequency current speed exceeded 25 cm/s (at ± 200 m below the surface), which occurred during eddy passages, the moorings were inclined considerably. The vertical position of the upper current meters could be up to 200 m lower than their upright position, as is observed from pressure sensors on the current meters. In case of these strong flows, the mooring also oscillated strongly, according to the strong pressure fluctuations. The frequency of these fluctuations was the semidiurnal tidal frequency. Also high-frequency oscillations of small amplitude may have been present, that are above the Nyquist frequency. The strong motion caused heavy damage to the rotors or interior of some of the current meters. During the second deployment period, for two moorings, the bottom weight was not heavy enough for the strong currents. Mooring ACS08 drifted some kilometers away from its original position. Mooring ACS06 even drifted more than 10 km to the southwest and was not detected during the recovery with the British RV Charles Darwin, but was found later after the mooring cable had broken and was then picked up. Because both the time resolution and the spatial coverage of the surviving current meters were better in the second deployment period, we will mainly consider these results.

Some current meters were provided with temperature sensors. In theory, temperature fluctuations can be directly related to the internal tide since the barotropic tide hardly causes excursions of the isotherms. But because of the mooring motion, temperature fluctuations may also be caused by the change in vertical position of the current meter. Separation of the two effects is cumbersome, if possible at all, therefore the temperature results are not used.

mooring position		water depth (m)	mooring ID	design depth (m)	instrument type	sampling rate hr ⁻¹	deployment period (yearday)
lat (S)	lon (E)						
16° 30.62'	39° 58.52'	536	ACS04-A	500	ADCP-LR	1	98-463
16° 24.73'	40° 16.63'	1595	ACS05-A	500	ADCP-LR	1	98-459
			ACS05-2	1498	RCM8	3	98-459
16° 41.92'	40° 48.41'	2199	ACS06-1	250	RCM8	3	98-460
			ACS06-2	400	RCM8	3	98-124
16° 48.74'	40° 48.41'	2603	ACS07-1	250	RCM8	3	99-464
			ACS07-2	400	RCM8	3	99-197
16° 58.63'	41° 56.02'	1998	ACS08-1	250	RCM8	3	99-457
			ACS08-2	400	RCM8	3	99-457
			ACS08-3	650	RCM8	3	99-457
			ACS08-4	1902	RCM9	3	99-457
17° 12.13'	42° 50.24'	1815	ACS09-1	350	RCM8	3	99-457
			ACS09-3	650	RCM8	3	99-457
17° 17.30'	43° 09.55'	445	ACS10-1	100	RCM8	3	99-305
			ACS10-2	200	RCM8	3	99-457
			ACS10-3	349	RCM8	3	99-457
16° 30.62'	39° 58.52'	526	ACS04-A	500	ADCP-LR	2	464-680
16° 24.73'	40° 16.63'	1595	ACS05-1	1000	RCM11	6	464-679
			ACS05-2	1498	RCM11	6	464-679
16° 41.92'	40° 48.41'	2199	ACS06-1	250	RCM9	6	467-750
			ACS06-2	400	RCM8	6	467-750
			ACS06-3	650	RCM8	6	467-750
16° 48.74'	41° 13.88'	2603	ACS07-2	400	RCM8	6	466-527
			ACS07-4	2507	RCM11	6	466-679
16° 58.63'	41° 56.02'	1998	ACS08-2	400	RCM8	6	466-680
			ACS08-3	650	RCM8	6	466-680
			ACS08-4	1901	RCM11	6	466-680
17° 12.13'	42° 50.24'	1815	ACS09-1	250	RCM8	6	468-677
			ACS09-2	400	RCM8	6	468-677
			ACS09-3	650	RCM8	6	468-677
			ACS09-4	1719	RCM11	6	468-677
17° 17.30'	43° 09.55'	445	ACS10-1	100	RCM9	6	468-615
			ACS10-2	200	RCM11	6	468-677
			ACS10-3	349	RCM8	6	468-677

Table 5.1: Position and sampling rates of the current meters that worked properly for more than 20 days. The second period is indicated separately, as different current meters were used and instrument losses occurred at different locations.

The horizontal velocity measurements were decomposed in two components: the u -component is directed along the mooring array, the v -component is perpendicular to it and in the direction of the channel. Thus the common geographical coordinate system is rotated clockwise over 14 degrees. The resulting u -components can then be compared directly with

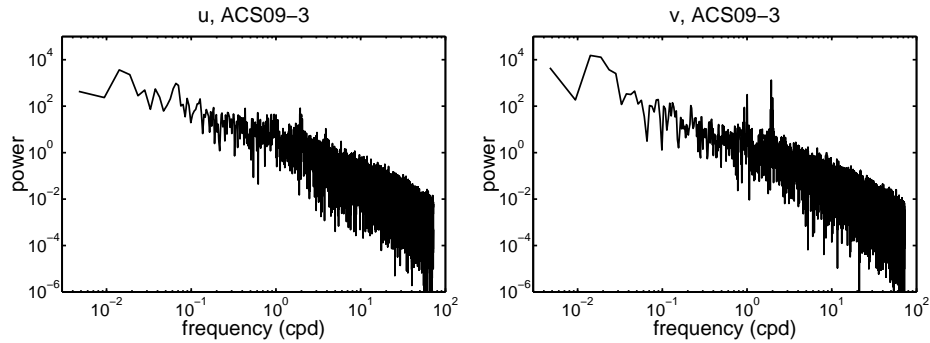


Figure 5.7: Raw power spectra ($\text{cm}^2 \text{s}^{-2} / \text{cpd}$) of ACS09-3, u in left panel, v in right panel.

the (two-dimensional) numerical models.

Spectra of the raw signal are shown in figure 5.7 for current meter ACS09-3, which serves as an example that exhibits features typical for this channel. The most energetic part is the low-frequency part, which must be associated with the eddies. The peaks of the tidal frequencies are much higher and sharper for the v -component than for the u -component.

5.5.1 Barotropic currents

To study internal tides, the barotropic tides have to be subtracted from the velocity records. We chose to estimate the barotropic currents from the data for every mooring separately. The time series were high pass filtered with a cut-off frequency of 1/4 cycle per day (cpd), to eliminate the energetic long-term flow (eddies). The filtered signals were averaged per mooring (vertical averaging). The upper current meters are more closely together and at first weight factors have been used to compensate for this. However, as this hardly altered the results, direct averaging was used.

Harmonic analysis was applied to the averaged velocity records to find amplitude and phase of the coherent tidal currents, according to

$$u = \sum_n U_n \cos(\omega_n t - \psi_n). \quad (2)$$

The tidal components that were taken into account are the diurnal components O_1 (soli-lunar declinational tide, period 23.93 hours) and K_1 (main lunar tide, period 25.82 hours) and the semidiurnal constituents N_2 (longer lunar elliptic, period 12.66 hours), M_2 and S_2 , as these five generally are strongest. Like for the yo-yo stations, the phase $\psi = 0$ refers to January 1st 2000 0 h00 UTC. It is assumed that the results represent the barotropic tide. The baroclinic tide should in theory be averaged out by averaging over the water column. Because of the poor vertical resolution, this might not be the case. However, internal tides are often intermittent (which is the case as will be illustrated), and they probably do not contribute significantly to the deterministic tidal part of the signal when long-term observations are analysed. The amplitudes and phases are displayed in table 5.2, for both periods (if available).

The time series of the high-passed, vertically averaged u -velocities were not well represented by the harmonic fit; the percentage of the signal that is accounted for by the analysis ranged from 30% to at most 50% for ACS08 and the ADCP near the shelf. For the individual current meters the fit was worse, 10% to 30%. The results were not consistent over the two periods of observation. The spectrum in figure 5.7 already indicated that the contribution of the tidal frequencies to the spectrum was small. Only in the ADCP's the vertically averaged tidal currents in u were significant. There the vertical averaging is more accurate, as nearly the whole water column is resolved.

The harmonic analysis of the v -component was more successful: 50% to even 80% of the signal was accounted for. The individual current meter signals close to the bottom were in general better represented by the harmonic analysis than those near the surface. Again averages gave better fits than individual records, but the differences are not as dramatic as for the u -component, pointing at the vertical persistence and dominant character of the v -component of the tidal currents.

The barotropic tidal flow due to the M_2 , S_2 and K_1 -tide dominated the current meter signal for the v -component. Amplitudes were not constant over the basin, tidal currents were weaker in the deeper parts of the basin and stronger near the shelf. Phases were nearly uniform for these components. Regarding the strong topography, that locally affects the currents, and the coarseness of the vertical resolution (especially at ACS06 and ACS07), which inhibited averaging out the internal tide in the vertical, the results seem consistent. The surface tide was determined from the pressure sensor on ACS04 and its decomposition is also included in table 5.2.

Hereafter the symbol \tilde{v} will be used for the v -component from which the barotropic tide has been subtracted. Then u and \tilde{v} are of the same order of magnitude in the semidiurnal tidal band. Because of the poor fit and low amplitudes, the fits were not subtracted from the u -component, except for the ADCP's.

5.5.2 Internal tides

Intermittency

To give an impression of the internal semidiurnal signal, band pass filtered (1.7-2.4 cpd) signals of u are presented in figure 5.8. Only the last mooring period is shown. The figure illustrates that the amplitudes were irregular. Near the shelf, motion was considerably stronger, which can be interpreted as the effect of the generation area where strong internal tides are expected. Events of high velocities of one current meter could not be related to events of high velocities in other current meter records. Since internal wave ray paths are different for the different tidal frequencies, at each current meter the internal waves will have different strength and phase, and will add up to different patterns (Gerkema, 2002).

But also for individual current meters velocity amplitudes were highly irregular (intermittent); the change in amplitude could not be attributed to a regular spring-neap cycle. This is typical for internal tides. In figure 5.9, u and \tilde{v} are plotted. Differences in phase and amplitude between the current meters were clearly present, but only for short time. They come and go. Also the phases and amplitudes of u and \tilde{v} varied with respect to each other for individual current meter records. Contrary to the mathematical definition of intermit-

mooring	O1	ψ	K_1	ψ	N_2	ψ	M_2	ψ	S_2	ψ	% fit
ACS04-I(<i>u</i>)	0.64	147	1.44	-108	0.49	166	2.32	64	1.05	-157	62
ACS04-I(<i>v</i>)	0.29	150	0.65	-112	0.33	167	1.34	72	0.58	-121	57
ACS04-II(<i>u</i>)	0.48	154	1.33	-101	0.33	144	1.47	91	0.88	-149	50
ACS04-II(<i>v</i>)	0.40	154	1.13	-101	0.39	-170	1.47	104	0.86	-123	52
ACS05-I(<i>u</i>)	0.30	-157	0.83	-79	0.56	-156	2.14	99	5.86	-74	43
ACS05-I(<i>v</i>)	0.51	162	1.20	-108	0.47	-87	1.52	108	0.63	-130	41
ACS05-II(<i>u</i>)	0.31	176	0.94	-95	0.40	150	0.81	90	0.43	-140	39
ACS05-II(<i>v</i>)	0.53	169	0.89	-80	0.79	-123	2.47	104	1.30	-86	73
ACS06-II(<i>u</i>)	0.27	169	0.24	-52	0.22	-158	1.29	105	0.63	-88	32
ACS06-II(<i>v</i>)	0.35	-168	0.81	-102	0.69	-124	2.29	128	0.90	-74	48
ACS07-II(<i>u</i>)	0.09	-63	0.46	-124	0.20	-78	0.72	88	0.29	-127	27
ACS07-II(<i>v</i>)	0.47	132	1.19	-93	0.26	178	2.41	99	1.37	-107	65
ACS08-I(<i>u</i>)	0.13	140	0.20	-140	0.09	95	0.37	113	0.21	-43	20
ACS08-I(<i>v</i>)	0.44	158	1.32	105	0.81	-134	2.25	98	0.91	-107	74
ACS08-II(<i>u</i>)	0.43	158	0.69	-84	0.40	-98	0.97	116	0.57	-109	50
ACS08-II(<i>v</i>)	0.58	175	1.17	-88	0.52	-142	2.25	108	1.21	-105	74
ACS09-I(<i>u</i>)	0.13	42	0.31	158	0.22	-58	0.42	-148	0.31	67	17
ACS09-I(<i>v</i>)	0.65	149	1.66	-117	0.74	-147	3.60	95	1.89	-110	75
ACS09-II(<i>u</i>)	0.31	7	0.48	175	0.25	-127	0.48	180	0.61	55	28
ACS09-II(<i>v</i>)	0.81	131	1.75	-113	0.66	-148	3.39	97	1.56	-116	85
ACS10-I(<i>u</i>)	0.40	-31	0.32	87	0.43	-15	0.52	144	0.44	-38	29
ACS10-I(<i>v</i>)	1.19	110	2.74	-127	1.29	-164	4.31	104	1.76	-120	77
ACS10-II(<i>u</i>)	0.52	-34	0.72	88	0.41	6	1.02	-174	0.71	17	32
ACS10-II(<i>v</i>)	0.89	117	2.81	-111	0.81	-96	3.62	98	2.07	-80	69
surface (m)	0.06	-148	0.05	-3	0.15	1	0.90	-105	0.49	67	98

Table 5.2: Harmonic analysis (amplitudes in cm/s, phases in degrees) of high pass filtered and vertically averaged current meter records, and harmonic analysis of depth sensor of ACS04 to give the surface tide (in m). Roman numerals indicate the period of observation: I is March/April 2000-2001, II is April-November 2001.

tency, where the presence of an intrinsic near-equilibrium causes near-periodic behaviour, it is here the constant perturbation in background conditions and forcing strength that causes the variability.

To quantify changes in amplitude and phase of current meter records, harmonic analysis was applied on windows of only four days of the band-pass filtered records shown in figure 5.8. For such narrow windows, the different semidiurnal constituents cannot be resolved. Therefore only M_2 was fitted, to represent the semidiurnal motion. The spring-neap cycle is then mimicked by a regular increase and decrease of the amplitudes and regular phase variations around a constant value. If the signal is dominated by M_2 , the fit to the windows is good, up to 100% for some windows. If the signal is dominated by S_2 , the phase may change dramatically and the fit is considerably less.

The results of harmonic analysis of the *u*-component of ACS09 and ACS10 are shown in figure 5.10 for four-day windows with steps of one day. The resulting amplitudes varied smoothly but irregularly. The signal, that was explained up to 30% by harmonic analysis

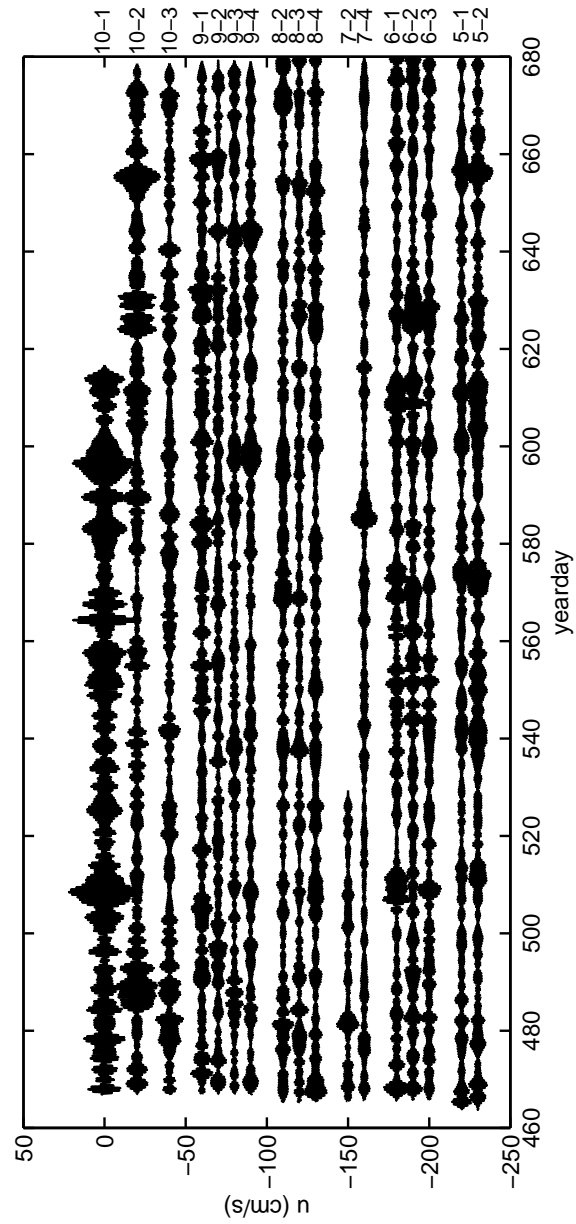


Figure 5.8: Observed band-pass (1.7-2.4 cpd) filtered u of current meters ACS05-ACS10. The vertical scaling is in cm/s, with offsets for the different records.

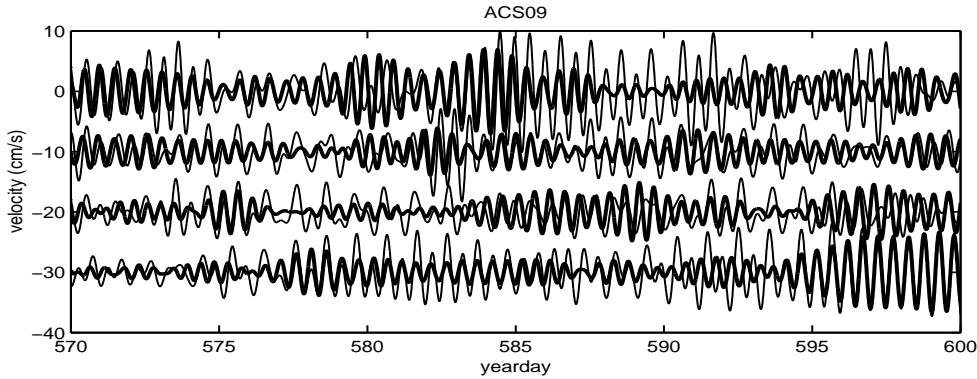


Figure 5.9: Enlargement of figure 5.8, that illustrates differences in the amplitude and phase in the vertical of the four ACS09 current meters for u (thick line) and \tilde{v} (thin line). The phase differences between the different current meter records for yearday 595-600 are especially clear, but phase differences can be found nearly at all times.

is now explained for generally more than 50% up to almost 100%. Most of the spikes in the phase are due to the transition of 180 to -180 degrees and vice versa, which is in fact a continuous transition.

Phases and amplitudes were different for the different current meters, which illustrates that we are looking at internal tides. For ACS09, current meters 1 and 2 in general had the same phase, current meter 4 was generally 180 degrees out of phase, current meter 3 tended to follow the upper two current meters, but differed considerably from time to time. Amplitudes of current meters 1 and 4 were largest. The lower current meter had small phase changes, whereas the upper current meter exhibited slow but large phase changes over the full 360 degrees and back. For ACS10-1 the upper current meter had the largest amplitudes. The phases of the three current meters were different, but those of 2 and 3 appeared more closely related. Also patterns of phase changes were different. For ACS10-1, the phase was generally around 170 degrees, with phase jumps due to the 180 to -180 degrees transition.

No direct relation was observed between amplitude and phase changes of the current meter internal tidal signal and the presence or absence of eddies, despite the changes in stratification and the mooring motion.

Spectra and integrated signal

As the internal tidal currents are highly variable, a different method is sought to quantify the overall results. The spectra appear a good instrument to do this. When the tidal signal is incoherent, due to changes in ray path or current meter position, the energy may leak to the side bands of the tidal bands (van Haren, 2002). Therefore the full semidiurnal band was studied.

Three different power spectra of u and \tilde{v} from different regions are shown in figure 5.11. The spectral levels in the generation area (ACS10-1) are clearly highest, also just outside the semidiurnal band. Peaks at the M_2 and S_2 frequency are visible, but do not stand out much.

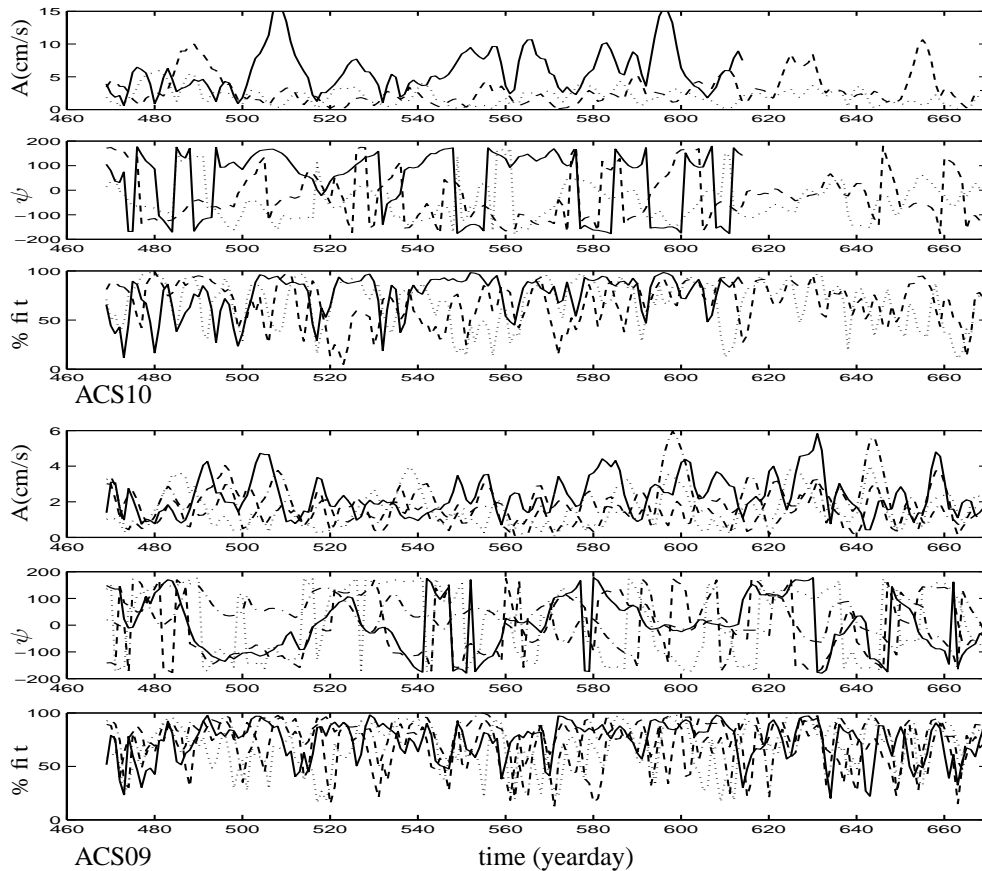


Figure 5.10: Fit of M_2 to band-pass filtered u -velocity in windows of 4 days with time steps of one day. From top to bottom: amplitude, phase and % fit of ACS10 (solid=upper, dashed=middle, dotted=lower current meter), amplitude, phase and % fit of ACS09 (solid=upper, dashed=second, dotted=third, dash-dotted=lower current meter).

In the spectrum of the near-bottom current meter ACS09-4 distinct tidal peaks are visible, which contain most of the energy. For this current meter, mooring motion can be neglected, variations must be attributed to changes in ray paths. Apparently amplitude and phase of the observed velocities did not change as much as in current meter ACS09-1, for which the tidal peaks have nearly vanished but for which overall levels are higher.

To enable the identification of regions where motion is strongest on average the spectra were integrated over the semidiurnal band. These results can then be compared with the numerical models. This is a coarse method, but it gives a summary of the different current meters results and eliminates the problem of the variability. The current meter records were high-pass filtered and the v -component was corrected for the barotropic tide. For the ADCP-records of ACS04-A and ACS05-A the spectra per bin were calculated and then averaged per

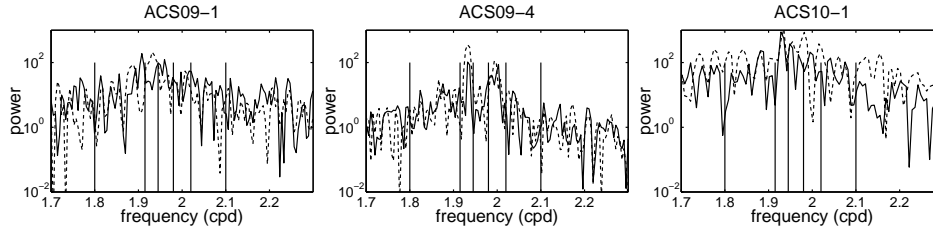


Figure 5.11: Power spectra ($\text{cm}^2 \text{s}^{-2} / \text{cpd}$) of u (solid) and \tilde{v} (dashed) for three different current meters. ACS10-1 is in the generation area, ACS09-4 is at the bottom and ACS09-1 at the top of a mooring. The vertical bars around 1.92 and 2 indicate the windows of intergration for the computation of the energy content of the M_2 and S_2 band, the outer vertical bars give the boundaries of the window for the semidiurnal band D_2 .

100 m. Mooring motion was not taken into account: for the ADCP's the vertical averaging already is a coarse approximation, for the current meters there is no way to correct for it. The full record length was used to get the best possible spectral resolution since also the integrals over small bands around M_2 and S_2 were computed. Using smaller windows and averaging did not alter the qualitative results for the total semidiurnal band, but the narrow bands were not resolved well. The contribution of the M_2 and S_2 -integrals to the total energy in the semidiurnal band is an indication for the variability of the tidal signal: a high contribution means that the periodic signal was persistent and that little energy has leaked to the sidebands. The results are put in table 5.3.

The table indicates that motion was strongest for the upper current meters of ACS04, ACS05 and ACS10. One may argue that the upper current meters near the shelf are in the generation area, but values of ACS05 are still strong, and this mooring is 40 km off the shelf. Further, this motion decreased rapidly with increasing depth. For the rest of the current meters, motion was strongest at ACS05-2, ACS06-2, ACS07-2, ACS08-4 and ACS09-1 for u , and for \tilde{v} at ACS05-2, ACS06-1, ACS07-2, ACS08-4 and ACS09-4. Differences between current meters remained however within a factor 4. The changes in location of maximum velocity of u and \tilde{v} may be caused by the subtraction of the barotropic tide for the latter. Subtraction of the true, vertically uniform barotropic tide should give the same maxima for u and \tilde{v} , as differences in the vertical are due to the baroclinic tide. As the vertical resolution is poor, the signal of one current meter may dominate, such that for this current meter \tilde{v} is lower and for the other current meters \tilde{v} becomes larger.

We will compare our results with the results from the numerical internal-tide generation model. The internal tidal current amplitudes and phases of u were calculated for the stratification with and without eddy and are displayed in plate VI. The two stratification regimes yield large scale patterns that are comparable, in the sense that for both stratification regimes, motion is strongest above the pycnocline. For the stratification with eddy, motion is generally weaker, which must be an effect of the change of wave ray direction with respect to the topography, which alters the effectiveness of internal-tide generation and focusing or defocusing upon reflection. Phase patterns are scattered more for the stratification with eddy, especially at the Madagascar side. The difference in pycnocline strength for the both regimes could be

ACS	u				\tilde{v}			
	M2	S2	K1	D2	M2	S2	K1	D2
04-50	6.6477	2.9538	0.7466	24.2471	2.2320	2.1607	0.6958	12.1404
04-150	2.3548	0.7576	0.3865	8.7603	1.0209	0.4133	0.5084	4.2808
04-250	1.2377	0.5321	0.4226	5.2019	0.3550	0.2738	0.2836	2.0029
04-350	1.2747	0.7976	0.5203	4.4088	0.6819	0.4233	0.4982	2.1551
04-450	1.7514	0.8369	0.3737	5.7101	0.6064	0.5233	0.3535	2.6209
05-50	5.3651	1.8222	1.5516	22.6459	4.4627	3.5676	1.9054	21.4495
05-150	2.9434	1.0444	0.6075	9.8855	1.5613	1.3873	1.2832	7.9199
05-250	2.6944	0.6564	0.7258	6.3895	0.9373	0.8655	0.7687	4.8273
05-350	2.3212	0.5621	0.8512	5.1309	0.4910	0.6356	0.6571	3.3653
05-450	1.9299	0.5175	0.5905	4.0469	0.3427	0.6015	0.5738	2.6479
05-1	0.5041	0.3806	0.6087	2.0203	0.3581	0.2292	0.1309	1.4075
05-2	1.0134	0.5779	0.7777	4.4001	0.3783	0.1295	0.2176	1.7126
06-1	0.6171	0.2323	0.3557	1.7950	2.6784	0.5454	0.3104	4.8952
06-2	1.0540	0.2634	0.2798	2.1940	0.8080	0.0984	0.2191	1.9261
06-3	0.8296	0.1578	0.2608	1.5176	0.2794	0.1305	0.4831	0.9139
07-2	0.5737	0.6064	0.2568	2.6448	0.1249	0.7508	0.0847	2.1412
07-4	0.4841	0.1540	0.1234	1.6296	0.2649	0.1341	0.2188	1.0937
08-2	1.0550	0.2126	0.5365	2.4047	0.2471	0.3364	0.2391	1.7814
08-3	0.1898	0.2906	0.5305	1.2730	0.1614	0.3514	0.3996	1.1273
08-4	1.4928	0.6501	0.6554	2.9928	0.1948	0.2884	0.1794	2.0150
09-1	0.3561	0.3979	0.2589	3.4636	1.4087	0.6752	0.2177	4.5477
09-2	0.2365	0.5690	0.5589	1.8848	0.5674	0.3441	0.3116	2.1277
09-3	0.3438	0.5651	0.3388	1.7861	0.0940	0.4804	0.3182	1.5092
09-4	0.6564	0.7843	0.5589	2.2867	3.9230	1.1794	0.2936	5.9214
10-1	6.5819	2.4783	1.4208	19.6943	3.1923	3.7489	2.1824	16.8149
10-2	0.9269	0.6453	0.4742	5.0844	1.9543	0.3587	0.7302	7.4445
10-3	0.4063	0.0943	1.6259	2.4360	1.8395	0.2781	0.0728	5.6944

Table 5.3: Spectral energy integrated over tidal bands for u and \tilde{v} , in $\text{cm}^2 \text{s}^{-2}$ for the second period of observations, except for ACS05-A. The numbers 50-450 refer to depths in m.

responsible for this (Gerkema, 2001). But also changes in ray paths may lead to different reflection patterns, with a different concentration of energy.

To compare, the energy in the semidiurnal band was transformed into overall semidiurnal band velocity amplitudes according to $A = 2\sqrt{(D_2\text{-integrated power})}$. The large values in the upper ADCP-observations and ACS10 are in accordance with the model. Especially the large values observed for ACS05-A, which is clearly outside the generation area, are reproduced as an effect of the the pycnocline.

Most current meters were not in these areas of strong motion, they are all well below the pycnocline. Still, there are differences in intensity of the currents, albeit not as large. For ACS09 the upper and lower current meter showed stronger motion, in accordance with the

model. This mooring was just to the south of the island Juan de Nova, that may generate internal waves also. Especially the \tilde{v} -component had large amplitudes. In ACS08 the strongest signal was found for the lowest current meter, although only for the u -component. Still, amplitude and phase differences between the current meters of this mooring were observed, indicating the presence of internal waves. Since motion was weak as compared to the other moorings, the results do not stand out. None of the three current meters were in positions where strong motion was predicted by the numerical model, the results seem consistent. ACS07 exhibited stronger motion for the upper current meter. This current meter is indeed close to a numerically predicted site of strong motion. For ACS06 the correction for the barotropic tide is doubtful, since the current meters may be within a single internal wave beam and vertical averaging may not rule this out. For \tilde{v} , the semidiurnal tidal energy is strongest in the upper current meter, for the u -component it is in the second current meter. This mooring has been displaced more than 10 km to the southwest by the currents. Inspection of the pressure sensor signals of the current meters suggests that this happened some weeks after the deployment. This may explain differences between observations and the model results. For ACS05, the u -component of the bottom current meter was stronger than for the current meter in the middle. In the model, the bottom current meter is indeed close to an area of stronger energy in the no-eddy stratification regime, but for the eddy regime the upper current meter is in an area of stronger motion. A semidiurnal internal wave beam, generated at the shelf, should reflect from the bottom at about this position as predicted by ray theory.

It is not possible to compare the phases of the integrated spectrum, as it was especially the variability of the phases that led to the use of an integrated spectrum. Phases of the short time harmonic analysis can be compared. For ACS09, the observed phase changes in the vertical are in accordance with the numerical model. The changes due to the presence and absence of an eddy lead to mild variations for the lower current meter, but to tremendous variations for the upper current meters. Also the relatively large contribution of the S_2 -component, as observed in the integrated spectra, could contribute to larger phase variations. For the lower current meters of ACS05, the phase changes (not shown) seemed to be relatively slow for large observational periods and the current meters generally had nearly equal phases, as predicted. For ACS10-1, the phase variations in time were relatively small (most jumps were due to the -180 to 180 degrees transition), which may be an effect of the coupling of the barotropic and baroclinic tides in the generation area. The model predicts large phase differences in the vertical, which are different for the two stratification regimes. These could be observed in the 10-2 and 10-3.

In general, the modelled variation of phase and amplitude in horizontal and vertical were large. Mooring motion alone could contribute very much to the intermittency, moving the current meter into and out of regions with strong motion, for example ACS05-1 and ACS08. Also phase changes may be considerable. In addition, the stratification changes nearly continuously due to the slow passage of eddies. Again for the current meters of ACS05 and ACS08-2 changes in phase and amplitude are particularly large. For S_2 , similar spatial variations of energy and phase were found from the numerical model. The combination of mooring motion, changes in stratification and the strongly localized regions with energy concentration or large phase jumps must lead to the observed intermittent behaviour.

5.6 Discussion

Internal tides were clearly present in the channel. Direct evidence came from the yo-yo stations, with isotherm displacements of 40 m to 80 m near the shelf. But they only provide a snapshot and are too far apart to be related to each other. Also differences in time with respect to spring time may contribute to amplitude differences.

The current meter observations presented here span a long time. The second period of observations was more successful in the sense that the time resolution and spatial coverage were better. Therefore, in the data analysis mainly results from the second period have been used, except for the ADCP off the shelf. However, the current meter signals reveal only highly variable internal tides, such that it is not possible to speak of *the* internal wave field. The intermittency makes it difficult to relate the signals of the different current meters. It is probably related to changes in wave ray paths due to the passage of eddies which alters the stratification, and changes in current meter positions due to large velocities of the eddies. Also Doppler shifts and changes in the absolute vorticity due to the large velocities in the eddies may put energy to nearby frequencies and alter wave ray paths (Kunze, 1985), but we did not take these effects into account, given other uncertainties. At some locations, the change in phase due to a change of ray path or mooring position may be particularly large, thus accounting for the intermittency (Gerkema, 2002). In this respect, the observations resemble the classical observations of Magaard & McKee (1973), who have long-time observations in the western North Atlantic, where eddies pass that are shed off by the Gulf stream. A direct connection between amplitude and phase changes of the internal waves and the passage of eddies was not found however. But also in shelf areas intermittency was observed (Lerczak *et al.*, 2003), albeit with a stable vertical structure. In van Haren (2002), the contributions of the different tidal frequencies M_2 , S_2 and N_2 could be separated in time and variations in their maxima could be interpreted as changes in ray path. Due to the strong mooring motion this is not possible here.

Calculation of the long-time energy content of the spectral bands of the semidiurnal frequency revealed that energy is concentrated around the pycnocline. This seems not purely an effect of the generation area, as it was also observed 40 km off the shelf. The pycnocline is assumed to play an important role in the behaviour of internal tides: for an intermediate strength waves are scattered whereas a strong pycnocline acts as a reflector such that an internal wave beam preserves its identity (Gerkema, 2001). The pycnocline was indeed rather strong. In the presence of an eddy it is considerably weaker. The exact generation locations and beam structure of the internal tides also seem closely related to the stratification (Gerkema *et al.*, 2003; Lam *et al.*, 2003).

None of the deep current meters revealed strong internal wave amplitudes. The presence of internal waves was however betrayed by phase differences between the current meters, as observed from the short term harmonic analysis of the filtered and barotropic tide-corrected records. Further, the strength of the velocity changed over the basin, maxima were reached at different moments in time, indicating different phases of the M_2 and S_2 tides at different locations.

The numerical internal-tide generation model was only valid for a cross section of an infinitely long channel. In reality, the Mozambique Channel is far from two-dimensional. The bottom topography in the along-channel direction is uniform along the Davie Ridge.

The island Juan de Nova, slightly to the north of ACS09 may generate waves that penetrate into our area of observation. Although the barotropic tide was strongest in the along-channel direction, no attention was paid to other generation areas. Finally, the fact that we observe in the narrowest part means that waves that propagate along the channel will be refracted away from this cross section upon reflection at the coast. This may be a serious limitation for the concentration of energy.

To conclude: internal tides were present, but the appearance for the individual current meters was highly intermittent. When long time averages of the signal were studied, it appears that the upper part of the water column contains the strongest internal tidal currents, but significant isotherm displacement was observed in the interior, where current meters were absent. It would be especially worthwhile to study internal wave currents in the upper few hundred meters, to investigate the effect of scattering and reflection near the pycnocline in more detail.

5.7 Synthesis

In relation to the rest of the thesis, it is clear that the observations cannot be interpreted as a simple wave attractor. This does not mean that the theory about wave focusing and the appearance of attractors is not applicable to the ocean at all.

The most important complication, that has not been discussed in previous chapters, is the effect of a strong spatial variation in stratification, which causes scattering, an effect that is not accounted for in ray theory. This has a large impact on the actual wave field, as shown by the numerical model. But also without scattering wave attractors cannot be readily found. Although internal waves with tidal frequencies are most easily generated, they do not necessarily lead to wave attractors, as the existence of wave attractors depends very much on the wave frequency. It is well possible that a basin of certain basin shape and stratification has potential for wave attractors for frequencies other than the tidal frequencies. Furthermore, in nature, basin shapes are hardly ever enclosed, such that part of the wave rays escapes to the shelf, or uniform in one direction, such that attractors cannot extend in the horizontal.

From the observational side, ocean observations only cover points, or lines for the ADCP's, whereas in the laboratory full cross sections could be observed. Unless a very good model is available and the observational programme is very well designed, interpretation of observations is difficult. Further, the variability in background conditions, resulting in the change of ray paths and therewith in intermittency, will complicate the detection of structure.

Still, the numerical tide generating model indeed showed that energy is distributed very unevenly, with patches of high concentration. Such patches cannot be predicted by low modes only, also high modes must be taken into account, as well as reflection at the bottom. The bottom topography is responsible for the generation, but it appears to determine the spatial distribution of wave energy as well. Despite the scattering, in the deep sea structures are very beam-like. This means that understanding reflection at the bottom remains an essential part of the understanding of inertial wave behaviour. It is very well possible that in the ocean "echoes" of internal wave attractors can be observed as isolated spots of high internal wave energy, that cannot be directly related to a generation area. In that respect, despite all its limitations, this thesis may contribute to understanding the behaviour of internal waves in oceans

and lakes.

This chapter is a manuscript by A.M.M. Manders, L.R.M. Maas and T. Gerkema. We thank H. Ridderinkhof for the realization of the observations and the crews of the Pelagia, Darwin and Bazaruto for their assistance.